On gravity currents over changing topography

M. Eletta Negretti, Jan-Bert Flòr and Emil Hopfinger

LEGI, CNRS
Grenoble
maria-eletta.negretti@legi.cnrs.fr

Abstract

We present experimental results on continuously supplied and well developed gravity currents moving from horizontal to concave or constant-slope boundaries. Results show that the gravity current velocity is in continuous spatial development and approaches an equilibrium state velocity only when the slope change is small. Following closely the theory of Turner (1973) we derive a general equation for the depth-integrated velocity including a variable slope angle and all forcing and dissipation sources. The comparison of this equation with the experimental data reveals that bottom friction can be very large in the region of appearance of the KH billows and of the same order of magnitude as entrainment. The comparison with currents on straight slopes reveals that the results are independent of bottom curvature and demonstrates that the current continuously adjusts to the gradual slope changes.

1 Introduction

Gravity currents are key features that affect ocean, atmospheric and coastal circulation (Baringer and Price (2001)). Ambient water and sediment from the bottom are entrained and mixed thus changing the properties of water masses.

Laboratory studies of gravity currents have been essential in the understanding of the dynamics of gravity currents. Most of these studies focused on gravity currents on horizontal or slightly inclined boundaries, where the head is an essential feature of the flow. The first experiments on a steady downslope flow were conducted by Ellison and Turner (1959) who also developed the, now classical, similarity theory of these flows (Turner (1973)). The initial developing region of an accelerating current over linear inclines (4° up to 15°), before reaching constant Richardson number conditions, was investigated by Pawlak and Armi (2001).

When there are rapid slope changes, the current may accelerate or decelerate which affects interfacial instability because of changes in the Richardson number and hence vertical mixing. In contrast with former studies, we consider a well developed horizontal flow, having a large Richardson number before reaching the concave or linear slope. The acceleration provoked by the abrupt slope change and consequent interfacial instabilities will cause strong entrainment of ambient fluid which rapidly slows down the current. The question is whether this flow still reach the expected equilibrium state on the slope, characterized by a nearly constant velocity due to a balance between buoyancy and total friction.

2 Theoretical analysis

We considered the general governing equation and then proceeded with the depth integrated equations following closely the procedure given in Turner (1973). The flow has

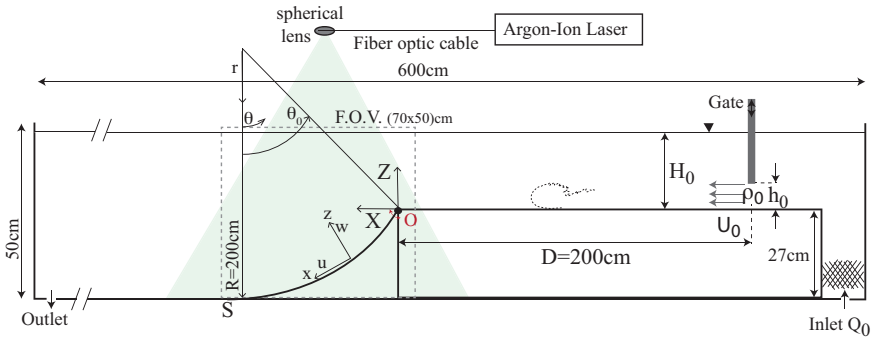

Figure 1: Sketch of the experimental set-up and definition of notations. We recall that $x = R(\theta_0 - \theta)$ and $z = (R - r)$.

been considered two-dimensional and stationary. Using the boundary layer and Boussinesq approximations and making use of the similarity hypothesis as in Turner (1973), after somme arrangements we obtain the following equation

$$\frac{U^3}{B} = \frac{\mathcal{S}_2 \sin\theta}{C_D + E\left(1 + \frac{1}{2}\mathcal{S}_1 Ri\right) + \frac{h}{U}\frac{dU}{dx}\left(1 + \frac{1}{2}\mathcal{S}_1 Ri\right) + \frac{1}{2}\mathcal{S}_1 h\frac{dRi}{dx}}. \tag{1}$$

Here, $Ri = \bar{g}' h \cos\theta / U^2$ is the bulk Richardson number with $\bar{g}' \cos\theta$ the buoyancy force normal to the wall, $B = \bar{g}' h U$ is the buoyancy flux per unit width which is constant and equal to the buoyancy flux supplied at the gate $B_0 = g'_0 h_0 U_0$, where U_0 and h_0 are the velocity and height at the gate. S_1, S_2 are factors related to the shape of the velocity and density profiles. For currents on slopes, typical values are $S_1 \approx 0.3$ and $S_2 \approx 0.8$, as also estimated from the current experiments. The first two terms in the denominator of (1) represent the total friction due to bottom drag (C_D) and interfacial entrainment (E), while the last term in the denominator represents the pressure variation along the slope. The third term represents the acceleration along the slope. Herein, we define an acceleration parameter $T_a = (h/U)dU/dx$, which can be either positive or negative as the pressure term.

A developed gravity current on constant slope moves at constant velocity (Ellison and Turner (1959), Britter and Linden (1980)). In this case (1) reduces to

$$\frac{U^3}{B} = \frac{\mathcal{S}_2 \sin\theta}{C_D + E}, \tag{2}$$

where terms in Ri have been neglected because $\frac{S_1}{2} Ri \ll 1$. The entrainment coefficient is now a function of slope angle only and can be approximated by $E = 9 \cdot 10^{-4}(\theta + 5)$ and when the slope angle $\theta > 5°$ bottom friction can be neglected. Thus, since $S_2 \sin\theta/\theta$ varies little in the range $10° < \theta < 50°$, the velocity is nearly the same on slopes in this range. This would suggest that on a varying slope boundary the velocity might remain constant provided it adjusts continuously to the varying acceleration.

3 Experimental set-up and inflow conditions

The experiments were conducted in an open glass-walled tank of approximately $6m$ long connecting two $800l$ reservoirs shown in figure 1. The channel cross section is reduced to $25cm$ wide and $20cm$ deep. The first section of the channel has a total length of roughly $2.3m$ (with the gate at $2m$ upstream), is horizontal and permits the boundary layer of the

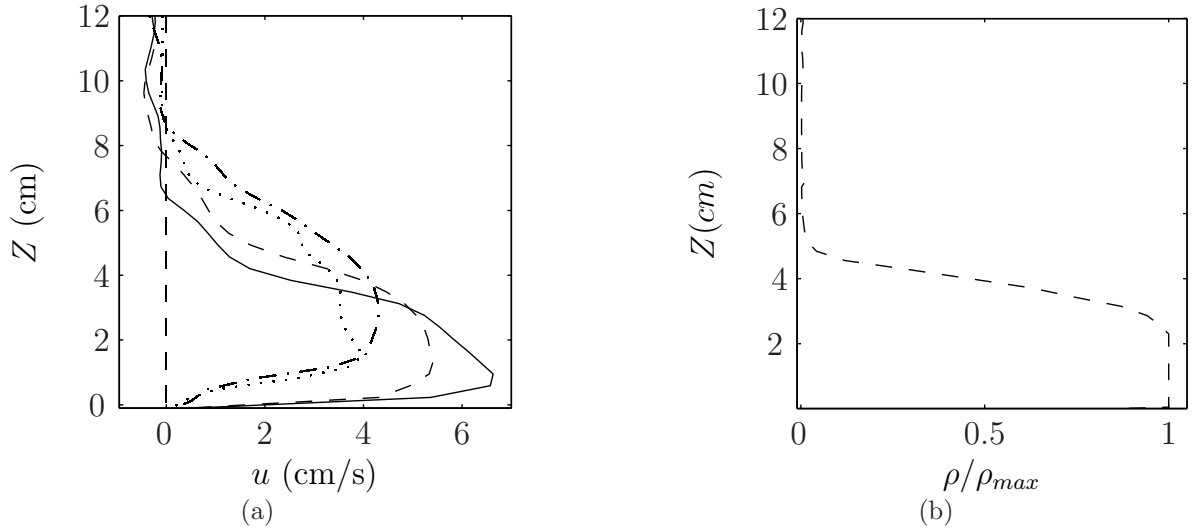

Figure 2: Initial conditions of the gravity current flowing on the initial horizontal channel. (a) Mean velocity profiles at $X = 20cm$ (....), 85 (−.), $195cm$ (−−) and $199cm$ (−) from the gate; (b) vertical density profile obtained from the dye visualizations at $D = 195cm$ from the gate for experiment C3.

gravity flow to fully develop. The next section is a concave or linear slope and is free to pivot about O (see figure 1) to vary $(H - H_0)$ and enables different starting angles θ_0 for the same radius of curvature $R = 2m$. The length $S = R\theta_0$ was varied in the experiments over concave slopes between $60cm$, $80cm$ and $110cm$ resulting in $\theta_0 = 17°$ (experiment C1), 23° (experiment C2) and 31.5° (experiment C3), respectively. On the concave wall the slope angle θ varies from the maximum θ_0 at the beginning of the slope to 0 at S (see figure 1). Additionally, two experiments over constant slopes with $\theta = 15°$ and 22° and lengths of respectively $S = 104cm$ and $S = 73cm$ have been performed.

The gravity current was generated pumping salt water at a given density ($g' = 4.5cm/s^2$) and flow rate ($Q = 0.6l/s$) from the first reservoir. The outlet is placed at the bottom of the downstream channel end to control the total water depth and allow to discharge the lower layer salty flow. Velocity measurements were made using the PIV technique with an acquisition frequency of 30 frames/s and a spatial resolution of $0.0435cm/pixel$. Dye visualizations using Rhodamine 6G were used to estimate the density profiles and some averaged values of the density field by normalizing locally with the maximal value. All averaged data presented are intended to be a time average over approximately 2,000 images except if specified differently.

The velocity and the current depth at $195cm$ downstream of the gate ($5cm$ before the slope change) have reached $U_m \approx 6cm/s$ and $h \approx 6cm$ respectively resulting in a bulk Reynolds number based on these scales of $Re = 3500$.

Figure 2a displays velocity profiles at $20cm$, 85, $195cm$ and $199cm$ from the gate. With increasing distance the shape of the profile approaches that of a wall jet.

The shape of the density profile can be estimated from the dye visualizations with Rhodamine 6G and is displayed in figure 2b at $195cm$ from the gate showing a top hat shape with a thin interface of $\approx 2cm$.

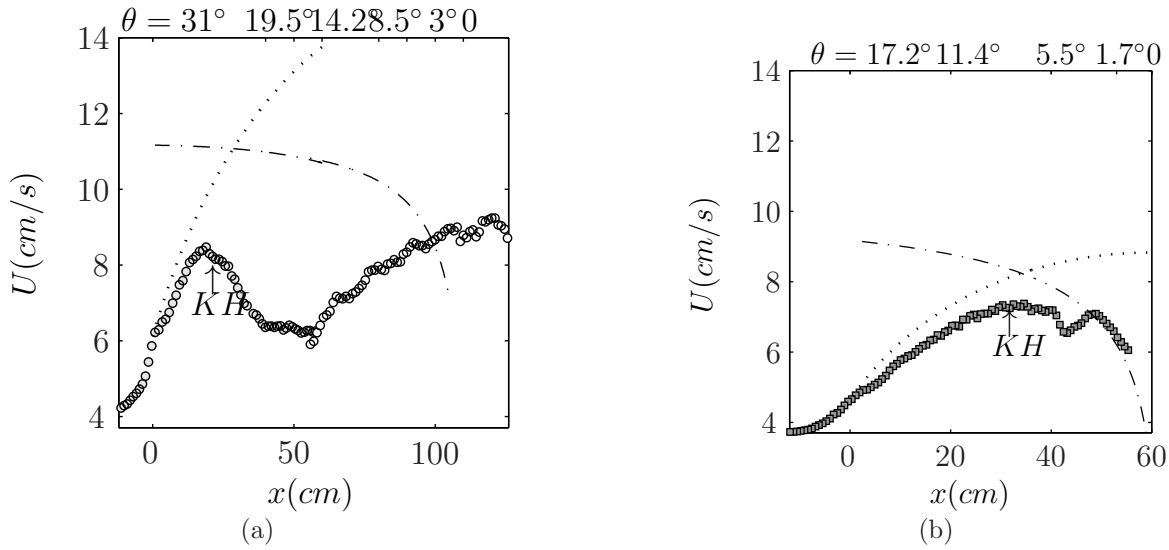

Figure 3: Comparison between experimental velocity (symbols) and the predictions of (2) (dash-dotted line) with $C_D = 2 \cdot 10^{-3}$ and $E = 9 \cdot 10^{-4}(5 + \theta)$ from Ellison and Turner (1959) for experiment C3 (a) and C1 (b). The dotted line represents the free fall solution neglecting friction and pressure variations.

4 Current on the concave slope

Figure 3 display the depth integrated experimental velocity (symbols) versus the downstream direction for respectively experiment C3 (a) and C1 (b). The dotted line represents the free fall velocity $U_{free} = \sqrt{2S_2 R g'_0(\cos\theta_0 - \cos\theta) + U_0^2}$, where the shape factor $S_2 = 0.75$ has been evaluated from the experimental data and U_0^2 is the velocity at the ridge $x = 0$. In experiment C3 the flow first accelerates, reaching a maximal value at $x \approx 17.5cm$, which corresponds approximately to the location where KH billows first develop. The velocity then decreases due to interfacial and bottom friction. After a re-adjustement, the velocity increases again at $x \approx 50cm$, where the slope is still 16°. At $x = 115cm$ ($\theta = 0$) the velocity seems to reach a value of $9cm/s$. At this location however, the flow has reached the end of the slope and it is expected to decelerate to find again the velocity $\approx \sqrt{2\overline{g'}h}$. This situation is very different from those normally described in previous studies of gravity currents: here, the flow, once on the slope, passes through acceleration-deceleration cycles before reaching the horizontal bottom at the end of the slope, where other conditions will dominate. The equilibrium state as in equation (2), in which the driving buoyancy force is balanced by the total friction (mainly due to entrainment), is here never reached. This is highlighted by comparing the measured velocities with the equilibrium state (2) indicated by the dash-dotted line in the figures 3a and b. Here the well-known entrainment law from Turner (1973) which can be fitted by $E \approx (5 + \theta°)9 \cdot 10^{-4}$ when $\theta > 5°$ has been used. Similar arguments hold for experiment C2. For both experiments C3 and C2, the maximal velocity is roughly 2/3 of the predicted equilibrium state velocity.

Experiment C1 behaves somewhat differently. We see from figure 3c that the velocity increases more gently until $x \approx 31cm$ corresponding again to the onset of the KH instabilities for this experiment. Then the velocity decreases again after a passage at a maximal value of $7.5cm/s$. This maximal velocity value is very close to the equilibrium state velocity of $8.4cm/s$. For $x > 50cm$, we observe an agreement between the equilibrium state

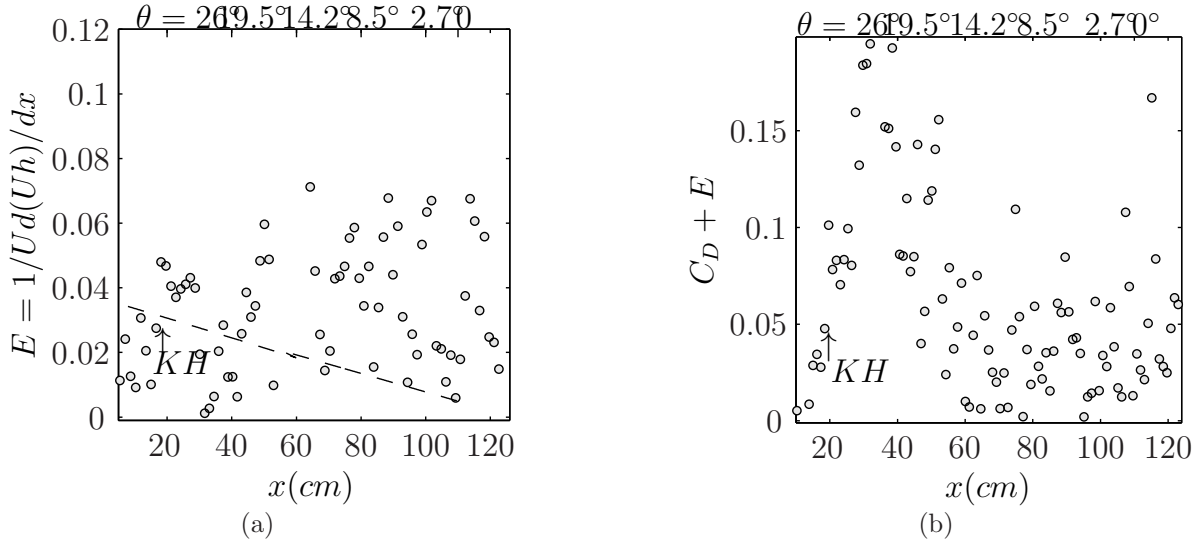

Figure 4: Entrainment coefficients $E = 1/Ud(Uh)/dx$ and total friction $(C_D + E)$ determined from equation (1) using the experimental data for experiment C3. $--$ $E = (5 + \theta)9 \cdot 10^{-4}$.

velocity and the experimental velocity, which are both decreasing rapidly.

In summary, we can state that when the initial slope angle is large the development of the gravity flow happens through acceleration and deceleration cycles. When the initial slope angle is small as for experiment C1, the acceleration is less and there is nearly a smooth approach of an equilibrium state.

It is clear that a smooth transition to an equilibrium flow governed by (2) requires that the initial acceleration of the current, expressed by an acceleration parameter, remains below a certain value. The local value of T_a,is not appropriate because it depends on the flow behaviour. We can introduce an overall acceleration parameter in the form $\overline{T_a} = h_i \Delta U/(U_m x_m)$, where x_m is the position of maximum velocity U_m , $\Delta U = U_m - U_i$ and h_i is the initial current height. In experiment C3, with $x_m = 17.5cm$, $U_m = 8.5cm/s$, $\Delta U = 2.5cm/s$ and $h_i = 5cm$, the value of this acceleration parameter is $\overline{T_a} = 0.07$. For experiment C1, $x_m = 31cm$, $U_m = 7.5cm/s$, $\Delta U = 2.5cm/s$ and $h_i = 4cm$, the value is $\overline{T_a} = 0.05$. These values are close to the local T_a estimated from the experiments.The implication is that for a smooth transition from U_i to an equilibrium velocity U_m the acceleration parameter needs to be $\overline{T_a} < 0.05$ but no critical value can be given. Low acceleration requires either a small slope or/and an interfacial instability near the beginning of slope change.

4.1 Entrainment

Given the velocity fields data, we can obtain estimates of the entrainment rates. The entrainment rate can thus be calculated from the variation of the flow rate observed in the experiments normalized by a local velocity relevant for the layer, i.e. $E = \frac{1}{U}\frac{dUh}{dx} = \frac{dh}{dx} + T_a$. The experimental entrainment rates for experiment C3 are presented in figure 4a. An alternative estimate of the entrainment rate can be made using equation (1). We can obtain a total friction coefficient $(C_D + E)$ by rearranging (1) equation in the form

$$C_D + E = \frac{\mathcal{S}_2 \sin\theta}{U^3/B} - T_a\left(1 + \frac{1}{2}\mathcal{S}_1 Ri\right) - \frac{1}{2}\mathcal{S}_1 h\frac{dRi}{dx} \tag{3}$$

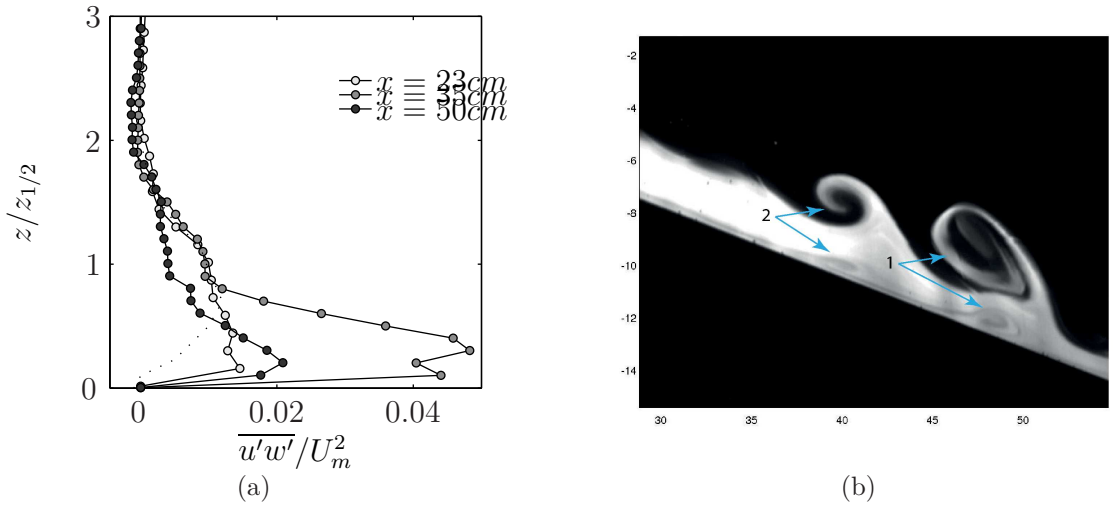

Figure 5: (a) Selected vertical velocity profiles of Reynolds stresses $\overline{u'w'}$ at three x positions on the concave slopes normalized with the maximal velocity U_m^2 for experiment C3. .... plane wall jet Zhou et al. (1996). (b) Zoomed views of the current at onset of KH instability of one experiment over straight slope ($\theta = 15°$), showing the development of large bottom billows coupled with the development of KH billows.

where the acceleration term, T_a, the change in Ri and the shape factor $\mathcal{S}_1$ are determined from the experiments. The extrapolated total friction coefficient is plotted in figure 4b. The comparison between the two figures allows an estimate of the bottom friction coefficient C_D and to verify the validity of the experimental entrainment coefficient E at the locations where $T_a = 0$ (the term of the variation of Ri is generally one order of magnitude less than the other terms and can thus be neglected). In figure 4a, we see that at $x \approx 20cm$ corresponding approximately to the location of onset of the KH instabilities, the entrainment coefficient is $E \sim 0.05$ and at the same location, the total friction coefficient is roughly the same. For $20cm < x < 30cm$ however, while the entrainment rates remain approximately $E \sim 0.05$, the total friction coefficient $(C_D + E)$ increases significantly with the largest values approaching 0.18. This implies (besides any source of experimental error, as for instance the power of 3 of the velocity in (3), the difficulties in determining T_a and the gradients of dRi/dx), that the bottom friction coefficient must become very large, of order 10^{-1} (figure 4b).

An estimate of the bottom friction coefficient C_D can be obtained from the velocity fluctuations in the boundary layer. Selected vertical profiles at different sections of the Reynolds stresses $\overline{u'w'}$ normalized using the local maximal velocity U_m are presented in figure 5a for the three experiment C3. The dotted line represents the measured values from Zhou et al. (1996) obtained for a wall jet. We see that in experiment C3 the values are very large as compared to the classical wall jet, reaching 5% of the maximal velocity.

This high shear stress is due to the particular development of the KH billows (merging process) which cause locally a significant decrease of the lower layer depth. Coupled with this phenomenon, we have also observed the generation of bottom billows in the bottom boundary layer rotating in opposite direction as compared to the KH billows. This is shown in figure 5b, which displays zoomed images of the dye visualizations in the regions of maximal bottom friction for one experiment over straight slope with $\theta = 15°$.

The question now is whether the current on straight slopes behaves similarly to that on

curved bottom. The large angle at the beginning and its following rapid decrease could cause the overshoot as the acceleration is inhibited by both the decreasing angle and the unstable interface, generating KH billows. We performed two additional experiments with a mean constant slope angle of 22° and of 15°. A very similar behavior as compared to the experiments over the concave bottom has been noticed. The depth integrated velocity behaves also very similar as for the curved boundaryand we observed the same behavior for the bottom friction coefficient and Reynolds stresses which presents very high values.

From this comparison we conclude that the slope curvature has apparently no effect on the spatial flow development.

5 Conclusions

The main results that emerge from the present study are: (i) when a gravity current with an initially stable interface on horizontal or a nearly horizontal boundary moves onto a steep slope, it undergoes a cycle of accelerations and decelerations and does not reach the constant equilibrium velocity within a distance of about $30h_0$ considered. (ii) The first KH billows cause boundary layer separation and reattachment that leads to a large boundary friction coefficient which is of the order of the interfacial drag due to entrainment. (iii) The spatial development on a concave boundary, more representative of natural slopes, is very similar to that on a constant slope boundary.

In order to make the results of more general interest, notably the velocity, it is appropriate to represent the development in terms of non-dimensional quantities. From (1) we get the velocity scale $(B_0 \sin\theta)^{1/3}$. An appropriate length scale is the distance x_c where KH instability is first observed and the current velocity reaches its maximum. This is related to a decrease in Richardson number down to a critical value Ri_c

$$Ri = \frac{g'h}{U^2}\cos\overline{\theta} = \frac{B_0}{U^3}\cos\overline{\theta} = Ri_c. \tag{4}$$

Using the free fall velocity $U_{free} = \sqrt{2g'_0 x_{c,th}\sin\overline{\theta} + U_0^2}$, where U_0 is the velocity at slope begin, we get an equation for $x_{c,th}$ as a function of the known initial parameters B_0, g'_0, U_0 and $\overline{\theta}$

$$x_{c,th} = \frac{\left(\frac{B_0}{Ri_c}\cos\overline{\theta}\right)^{2/3} - U_0^2}{2g'_0\sin\overline{\theta}}. \tag{5}$$

For the critical Richardson number we take the experimental value of $Ri_c = 0.13$ at onset of KH instability and on the concave boundary we take for the slope angle $\theta = \overline{\theta}$, that is a mean slope between $x = 0$ and x at KH instability onset. The theoretical predictions for $x_{c,th}$ are in good agreement with the experimental observations of $x_{c,exp}$ for all experiments.

In figure 6b the depth integrated velocities for all experiments using $x_c \equiv x_{c,exp}$ to normalize the downstream direction x and using $(B_0 \sin\overline{\theta})^{1/3}$ to normalize the velocity U are plotted. We see that the velocity data nicely collapse on a single curve $x/x_c \leq 1$, with a non-dimensional velocity maximum of about 2.6. Different decays are observed for $x > x_c$ for the different experiments, including experiment C1, where an overlap between the equilibrium state velocity and the experimental velocity has been highlighted in § 4 (cf. figure 3b) close to the end of the slope, where bottom drag starts to be dominant. The first

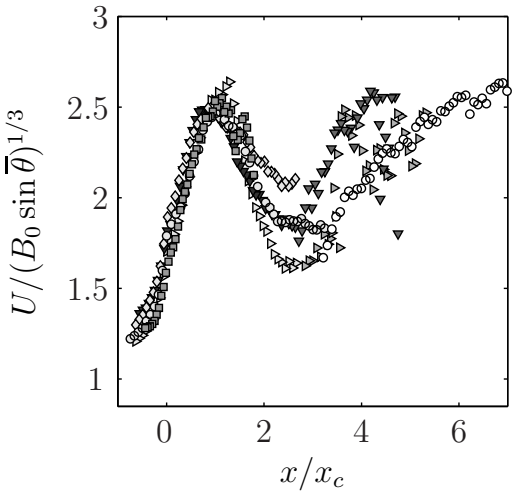

Figure 6: Depth integrated velocity normalized by $(B_0 \sin\overline{\theta})^{1/3}$ along the downstream direction normalized by $x_c \equiv x_{c,exp}$ for all experiments on concave and straight slopes.

velocity minimum is at $x/x_c \approx 2.5$. An overall acceleration parameter $\overline{T_a} = \frac{h_i}{U_m}\frac{\Delta U}{x_m}$ has been defined with $\overline{T_a} \geq 0.05$ for currents with strong velocity oscillations, and a smooth transition for $\overline{T_a} < 0.05$.

The high values of C_D obtained from velocity data are consistent with the observed values of the Reynolds stresses in the boundary layer, reaching values of $\overline{u'w'}/U_m^2$ of 5 to 8%. These are much larger and are closer to the bottom boundary as compared to classical wall jets. Dye visualizations have shown the continuous formation of billows ($1cm$) in the bottom boundary layer coupled with the development of the large KH billows at the interface (figure 5b). The small billows in the boundary layer are characteristic of boundary layer separation.

References

Baringer, M. and Price, J. (2001). Mixing and spreading of the Mediterranean outflow. *J. Phys. Ocean.*, 27:1654–77.

Britter, R. and Linden, P. (1980). The motion of the front of a gravity current travelling down an incline. *J. Fluid Mech.*, 99(3):531–543.

Ellison, T. and Turner, J. (1959). Turbulent entrainment in stratified flows. *J. Fluid Mech.*, 6(3):423–448.

Pawlak, G. and Armi, L. (2001). Mixing and entrainment in developing stratified currents. *J. Fluid Mech.*, 424:45–73.

Turner, J. (1973). In *Buoyancy effects in fluids*, pages –. Cambridge University Press.

Zhou, M., Heine, C., and Wygnanski, I. (1996). The effect of excitation on the coherent and random motion in a plane wall jet. *J. Fluid Mech.*, 310:1–37.